Journal of Power Sources 196 (2011) 1615–1619

Contents lists available at ScienceDirect

Journal of Power Sources

journal homepage: www.elsevier.com/locate/jpowsour

Short communication

Hierarchical porous carbons prepared by an easy one-step carbonization and activation of phenol–formaldehyde resins with high performance for supercapacitors

Zhoujun Zheng [a], Qiuming Gao [a,b,*]

[a] State Key Laboratory of High Performance Ceramics and Superfine Microstructures, Graduate School, Shanghai Institute of Ceramics, Chinese Academy of Science, 1295 Dingxi Road, Shanghai 200050, PR China
[b] School of Chemistry and Environment, Beihang University, 37 Xueyuan Road, Haidian District, Beijing 100191, PR China

ARTICLE INFO

Article history:
Received 18 December 2009
Received in revised form 26 August 2010
Accepted 7 September 2010
Available online 15 September 2010

Keywords:
Hierarchical porous carbon
Phenol–formaldehyde resin
Simple preparation
Supercapacitor

ABSTRACT

Hierarchical porous carbons are prepared by an easy one-step process of carbonization and activation derived from phenol–formaldehyde resins, in which potassium hydroxide acts as both the catalyst of polymerization and the activation reagent. The simple one-step preparation saves the cost of carbons and leads to high yield. The porous carbons have high surface areas with abundant pore structures. The plenty of micropores and small mesopores increase the capacitance and make the electrolyte ions diffuse fast into the pores. These hierarchical porous carbons show high performance for supercapacitors possessing of the optimized capacitance of 234 F g^{-1} in aqueous electrolyte and 137 F g^{-1} in organic electrolyte with high capacitive retention.

1. Introduction

Supercapacitors, also called electrochemical capacitors, can supply high power energy in short time, which meet the requirements of the applications for hybrid electric and fuel cell on-board vehicles [1]. They are also widely used in portable devices such as cell phones, cameras, video recorders and cordless tools [2]. Transition-metal oxides, conducting polymers and carbon materials [1] are the fundamental candidates for supercapacitor electrode materials. Among the available metal oxides, RuO_2 shows an excellent performance due to its good conductivity and three distinct oxidation states accessible within 1.2 V [1]. But it is limited applied in commercial use because of the high cost. Other cheaper metal oxides such as NiO suffer from low voltage windows and poor conductivity [3]. Conducting polymers have short cycle life as the electrodes despite of high capacitance [4]. As a consequence, porous carbon materials turn out to be the most promising candidate for supercapacitor electrodes because of the high conductivity, electrochemical stability, open porosity and low cost [4–6].

In the recent years, activated carbons, carbide-derived carbons (CDCs) [7], templated carbons [8] and carbon nanotubes [9] have been investigated for electrochemical double layer capacitors (EDLCs). The capacitance of EDLC is due to the separation and specific surface area (SSA) [10] according to the equation (1):

$$C = \frac{\varepsilon_r \varepsilon_0 A}{d} \quad (1)$$

where, ε_r and ε_0 are the electrolyte dielectric constants, A is the electrode surface area, and d is the separation between electrolyte ions and carbon. According to the equation above, the carbon materials with high surface areas and proper pore structures are suitable for the EDLC electrodes. Although the templated carbons and carbon nanotubes have excellent performance for the EDLCs, they do not satisfy the requirement of commercial application because of their complicated preparation and the relatively high cost [11]. On the contrary, activated carbons are the most common used materials because of their high surface areas and low cost. Activated carbons can be derived from natural materials (coconut shells, wood and coal) or synthetic materials (polymers) by carbonization in inert atmosphere followed by activation via KOH, CO_2 or steam vapor. Although the activation after carbonization increases the SSAs of the carbons, it leads to wide pore size distribution and low production yield. Therefore, designing carbon materials with suitable pore size distribution by simple method is a major research objective for the application of activated carbons for EDLCs.

Herein, we report a simple preparation of hierarchical porous carbons by carbonization and activation in one step. The porous carbons are carbonized and activated in the same step in inert

* Corresponding author at: School of Chemistry and Environment, Beihang University, 37 Xueyuan Road, Haidian District, Beijing 100191, PR China.
Tel.: +86 10 82338162; fax: +86 21 52413122.
E-mail addresses: qmgao@buaa.edu.cn, qmgao@mail.sic.ac.cn (Q. Gao).

0378-7753/$ – see front matter © 2010 Elsevier B.V. All rights reserved.
doi:10.1016/j.jpowsour.2010.09.010

atmosphere by contrast with the two separate step preparation of common porous carbons. Therefore, these hierarchical porous carbons have higher yield and relatively lower cost. According to the nitrogen adsorption–desorption isotherms in liquid nitrogen, the porous carbon activated by five amounts of KOH shows high surface areas with proper porosity. The abundant micropores increase the SSA of the carbon and the micropores match the electrolyte ions, which increase the capacitance. Moreover, the small mesopores generated in the activation favor the fast diffusion of electrolyte ions into the pores [12]. As a result, the porous carbon maintains high capacitive performance at high current density.

2. Experimental

2.1. Synthesis of the hierarchical porous carbons (HPCs)

In a typical synthesis, 1.1 g of phenol and 3/5 g of KOH were dissolved in 30 g of ethanol (named as HPC-3 and HPC-5). Then, 2 mL of 40% formaldehyde aqueous solution was added into the mixture. The mixture was stirred at 80 °C for 2 h and dried in oven at 100 °C over night. The light yellow mixture was transferred into an alumina boat and heated at 750 °C for 1 h in nitrogen with a heating rate of 1.5 °C min^{-1}. After cooling down to room temperature, the sample was washed with deionized water thoroughly to remove the excess alkali and dried in oven at 80 °C.

2.2. Synthesis of ordered mesoporous carbon CMK-3 activated by KOH (CAs)

The mesoporous carbon CMK-3 was synthesized from SBA-15 using sucrose as carbon precursor. The detailed preparation can be found in the literature [8]. The activation of CMK-3 was as followed. In a typical synthesis, 1 g of CMK-3 was impregnated with a KOH solution containing 3/5 g of KOH (named as CA-3 and CA-5). After dried in oven at 100 °C over night, the mixture was transferred into an alumina boat and heated at 750 °C for 1 h in nitrogen with a heating rate of 1.5 °C min^{-1}. The sample was washed with deionized water and dried in oven at 80 °C.

2.3. Synthesis of the activated carbon by general KOH activation of phenol–formaldehyde (PF) resin

The synthesis route of PF was according to the literature [13]. The weight ratio of KOH/PF was chosen as 5:1. The activated process was heated at 750 °C for 1 h in nitrogen with a heating rate of 1.5 °C min^{-1}. And the sample was washed with deionized water and dried at 80 °C.

2.4. Characterization

Nitrogen adsorption-desorption isotherms at 77 K and CO_2 adsorption measurements at 273 K were measured on a Micromeritics ASAP 2020 instrument. Electrochemical measurements were conducted on CHI-440a and Land CT2001a electrochemical testing systems. The samples were grounded with 10 wt.% of polytetrafluoroethylene binder and 10 wt.% of carbon black. The grounded powders were pressed between two pieces of nickel foams. After vacuum overnight at 100 °C, the electrodes were impregnated with 6 M KOH or 1 M NEt_4BF_4. The two electrode systems were used in cyclic voltammetry and charge–discharge measurements. 10 mg of the porous carbons were contained in the electrodes.

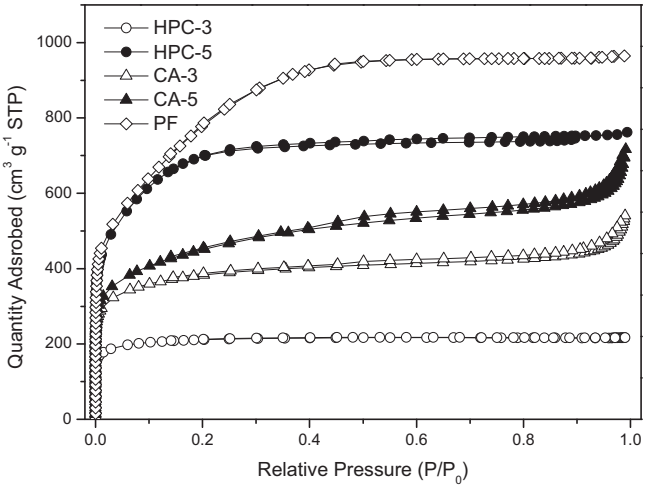

Fig. 1. N_2 adsorption–desorption isotherms of the HPCs, CAs and PF at 77 K.

3. Results and discussion

3.1. One-step preparation of HPCs

KOH-activated carbons can be synthesized from coals, pitches, fruit shells, woods, polymers and ordered mesoporous carbons. Among these processes, the yields of activated carbons derived from coals are relatively high because of the high carbon contents of the precursors. For example, the activated carbon fiber derived from coal tar pitch has a yield from 27 to 47% [14]. The yields of activated carbons derived from lignocellulose and polymer precursors are about 15–20% [15–18]. The yield of PF here used as comparison is 20%. KOH activations of ordered mesoporous carbons are also commonly used to improve the pore structures and electrochemical properties. The yields of the activated carbons are low, such as CMK-3, the yield is less than 30%. Furthermore, the ordered carbons require extra steps to prepare scaffolds and sacrificial use of not only the scaffolds but also the surfactants [19] which makes the synthesis complicated and increases the cost. Compared with the methods above, the synthesis process of HPCs is quite simple. The phenol and formaldehyde are polymerized at the presence of KOH as catalyst in ethanol. After dried in oven to remove the solvent of ethanol, the mixture of resol and KOH was directly carbonized, that is different from the normal preparation of the porous carbon using resol as the precursor. The KOH in the processes acts as not only the catalyst of polymerization, but also the activation reagent for the activation together with the carbonization. The method of carbonized and activated in the same step prevents twice heating of the carbon and saves the energy and cost. As a consequence, the yields of the HPCs are high with the values of 54% and 27% for HPC-3 and HPC-5. The yield is also higher than that of CDCs such as TiC-CDC (the theoretical yield of TiC-CDC is 20% according to the molecule weight) [10].

3.2. Structure analysis

As shown in Fig. 1, the nitrogen adsorption–desorption isotherms of the HPCs are close to type-I, indicating that the HPCs are mainly microporous characteristics. CAs and PF are chosen to compare with HPCs. The isotherm of HPC-5 shows a small hysteresis loop at medium relative pressure, which is due to the presence of mesopores in the carbon framework. The isotherms of CAs are similar and close to type-IV. Their surface areas are between HPC-3 and HPC-5. The isotherm of PF is close to type-I and it has the largest surface area among the samples. The pore structure parameters of the

Table 1
The texture properties of the HPCs, CAs and PF.

Samples	S_{BET}[a] ($m^2\ g^{-1}$)	S_{mic}[b] ($m^2\ g^{-1}$)	S_{CO_2}[c] ($m^2\ g^{-1}$)	V_{total}[d] ($cm^3\ g^{-1}$)	V_{mic}[e] ($cm^3\ g^{-1}$)	V_{CO_2}[f] ($cm^3\ g^{-1}$)	D_{mic}[g] (nm)
HPC-3	758	756	1400	0.33	0.30	0.46	0.52
HPC-5	2445	2388	3886	1.17	0.73	1.60	0.70
CA-3	1365	846	–	0.81	0.53	–	0.56
CA-5	1584	638	–	1.06	0.59	–	0.61
PF	2653	2481	–	1.26	0.80	–	0.75

[a] Brunauer–Emmett–Teller (BET) surface area.
[b] Micropore surface area, derived from the *t*-plot method.
[c] Micropore surface area, derived from the Dubinin–Astakhov method with CO_2.
[d] Total pore volume, measured at $P/P_0 = 0.98$.
[e] Micropore volume, derived from the Dubinin–Astakhov method.
[f] Micropore volume, derived from the Dubinin–Astakhov method with CO_2.
[g] Micropore average diameter, calculated by the Horvath–Kawazoe method.

HPCs, CAs and PF are all listed in Table 1. For HPC-3, the V_{micro}/V_{total} is 91%, indicating that it is close to an absolute micropore structure. In the case of HPC-5, the V_{micro}/V_{total} is 62%, which is in accordance with the result presented in Fig. 1 that HPC-5 has some mesopores besides the large amounts of micropores. The BET surface area and total pore volume of HPC-3 is 758 $m^2\ g^{-1}$ and 0.33 $cm^3\ g^{-1}$. With the increase of the mass ratio of KOH to carbon from 3 to 5, the micropores grow in large quantities. The pore size of micropores increases a bit, which leads to the formation of small mesopores from micropores. As a consequence, HPC-5 shows much higher BET surface area and larger pore volume of 2445 $m^2\ g^{-1}$ and 1.17 $cm^3\ g^{-1}$. Likewise, the BET surface area and total pore volume of CAs increase from 1365 $m^2\ g^{-1}$ and 0.81 $cm^3\ g^{-1}$–1584 $m^2\ g^{-1}$ and 1.06 $cm^3\ g^{-1}$ with the increase of KOH (Table 1). However, the changes of BET surface and pore volume are smaller than those of HPCs. And the micropore surface areas of CAs decrease during this process. This may be due to the fact that the small micropores grow larger when the mass ratio of KOH increases. PF shows the largest BET surface area and total pore volume of 2653 $m^2\ g^{-1}$ and 1.26 $cm^3\ g^{-1}$. Both HPC-5 and PF are activated by 5 weight amount of KOH. However, PF shows the higher degree of KOH activation. It is due to that KOH plays a different role during the synthesis. In the case of HPC-5, KOH acts as both catalyst and activation reagent. As a result, KOH is consumed partly before the activation process which leads to that the surface area and pore volume of PF are a bit higher than that of HPC-5.

Fig. 2 shows the micropore and mesopore volume distributions of the HPCs, CAs and PF calculated by the density functional theory (DFT) method, which also confirms the KOH activation process. HPC-3 and CA-3 show narrow micropore size distributions at about 0.52 nm and 0.56 nm. The micropores less than 1 nm of HPC-5 increase a bit compared with that of HPC-3. However, the micropores and small mesopores between the pore sizes from 1 to 3 nm of HPC-5 are generated a lot. Correspondingly, the total pore volume and the volume of micropore of HPC-5 increase to 1.17 and 0.73 $cm^3\ g^{-1}$. And the average micropore size of HPC-5 shifts to 0.70 nm. By contrast with the increase of micropore and small mesopore for HPC-5, the obvious pore volume increase for CA-5 is mainly in the mesopore range from 2 to 4 nm. Therefore, the increase of surface areas of HPCs is apparently higher than those of CAs when the value of KOH increases. All these phenomena are due to the fact that with the degree of KOH activation increasing, many micropores are formed in the carbon frameworks and the existing micropores grow larger leading to the formation of small mesopores. In the case of PF, the micropore distribution is close to that of HPC-5. The difference between PF and HPC-5 is that PF has larger mesopores and the average pore size is bigger than that of HPC-5. This is in accordance with the higher KOH activation degree of PF. Correspondingly, the average micropore size of PF is 0.75 nm and it shows a lot of mesopores between 2 and 4 nm which are all a bit larger than that of HPC-5.

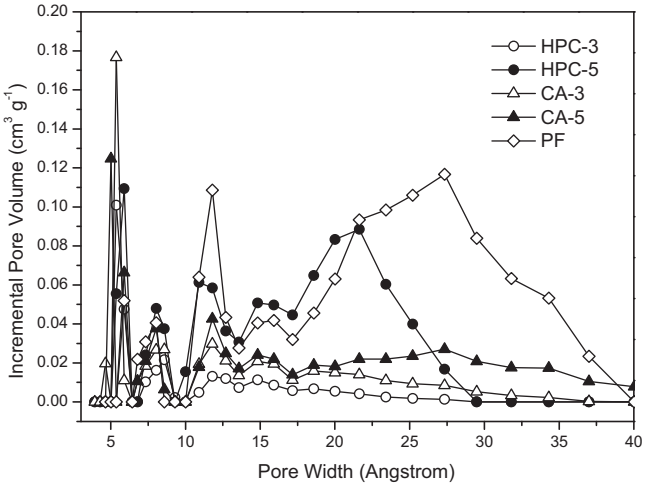

Fig. 2. Micropore and mesopore volume distribution calculated using the DFT method.

Moreover, because the HPCs show typical micropore structures, the CO_2 adsorption isotherms of the HPCs at 273 K were measured to ensure that the gas entered the very small micropores without kinetic limitation. According to the data of CO_2 adsorption listed in Table 1, with the amount of KOH increasing, large amounts of small micropores are formed. As a result, the micropore surface area of HPC-5 calculated derived from CO_2 adsorption increases a lot compared with that of HPC-3. This phenomenon agrees well with the result derived from the N_2 adsorption.

3.3. Property determination

Figs. 3 and 4 display the cyclic voltammograms of the HPCs at 2 mV s^{-1} in aqueous electrolyte and organic electrolyte. The cyclic voltammograms in 6 M KOH solution are shown in Fig. 3. The HPCs show good capacitance due to the abundant micropores in the structures. The voltammograms are close to rectangular shapes which indicate that the HPCs act as EDLCs in aqueous electrolyte. The integral area of voltammogram of HPC-5 is larger than that of HPC-3, which is in accordance with the higher surface area of HPC-5 compared with that of HPC-3. The data of specific capacitances of HPCs, CAs [20] and PF in 6 M KOH electrolyte calculated from cyclic voltammograms are listed in Table 2. Both HPC-5 and PF show good capacitance values at the scan rate of 2 mV s^{-1}. Based on the analyses of the data in Tables 1 and 2, we can find that the capacitance values have linear relationships with the SSAs. The V_{meso}/V_{total} of CA-5 is 44% calculated from Table 1, which is a bit larger than those of HPC-5 and PF. As a result, CA-5 offers the more paths for the

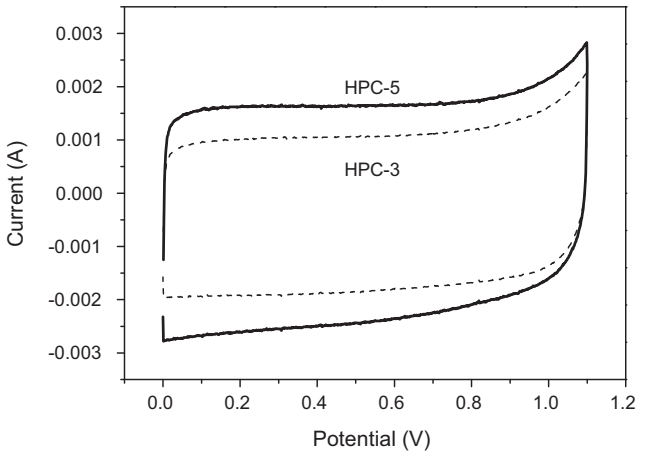

Fig. 3. Cyclic voltammograms of the HPCs in 6 M KOH at the scan rate of 2 mV s^{-1}.

Table 2
The specific gravimetric capacitance of the HPCs, CAs and PF in 6 M KOH electrolyte at different scan rate.

Samples	Specific capacitance (F g^{-1})				
	2 mV s^{-1}	5 mV s^{-1}	10 mV s^{-1}	20 mV s^{-1}	50 mV s^{-1}
HPC-3	157	144	130	123	121
HPC-5	212	198	189	181	172
CA-3	178	173	169	163	157
CA-5	197	191	186	180	173
PF	220	205	196	181	151

diffusion of electrolyte ions, which leads to a better capacitance retention at high scan rate than HPC-5.

The behavior of the HPCs in organic electrolyte is rather different from that in aqueous electrolyte. As presented in Fig. 4, HPC-5 maintains good capacitance performance in 1 M NEt_4BF_4 electrolyte. However, HPC-3 shows poor capacitance behavior. This is result from the follow facts. First, there are fewer micropores presented in HPC-3. The surface area of HPC-3 is only about one third of that of HPC-5 as shown in Table 1. According to Eq. (1), the specific capacitance has a linear relation with the SSA. Therefore, the capacitance of HPC-3 in organic electrolyte is smaller than that of HPC-5. The specific capacitance of HPC-5 in organic electrolyte is 137 F g^{-1}; however, the capacitance of HPC-3 is only 45 F g^{-1}. The result agrees with the analysis according to Eq. (1). Second, the average pore size of HPC-3 is only 0.52 nm. The small micropores block the diffusion of the organic electrolyte ions [21]. The

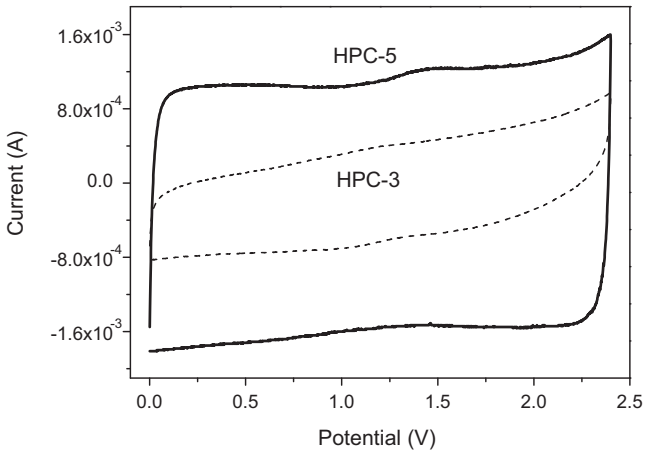

Fig. 4. Cyclic voltammograms of the HPCs in 1 M NEt_4BF_4 at the scan rate of 2 mV s^{-1}.

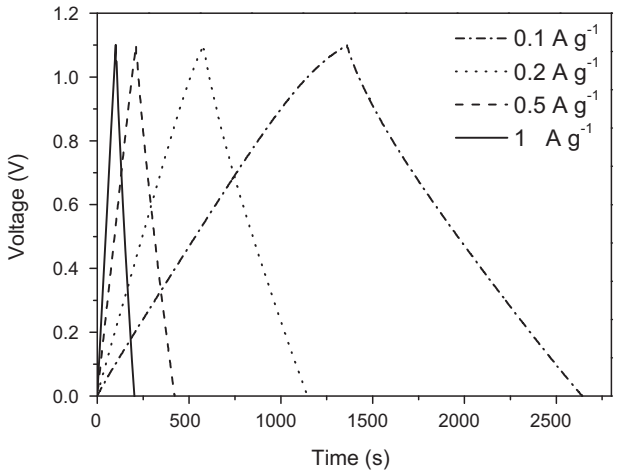

Fig. 5. Charging/discharging curves of HPC-5.

SSAs attributed to the small micropores have no contribution to the capacitance, which results in the decrease of capacitance in organic electrolyte. On the contrary, the pore size of HPC-5 is suitable for the organic electrolyte ions. The micropores in HPC-5 (0.70 nm) match the desolvated organic cations (0.67 nm) [21], which leads to good EDLC performance [10] in organic electrolyte. Furthermore, the small mesopores besides the micropores in the carbon framework of HPC-5 provide fast diffusion channel for electrolyte ions, which increases the capacitive performance of HPC-5.

Fig. 5 is the example of charge/discharge curves of HPC-5 from 0.1 to 1 A g^{-1}. The curves show isosceles triangle shapes, which indicate the stability and reversibility of the capacitance. The specific capacitance of the HPCs can be calculated according to the following equation [22]:

$$C = \frac{2It}{Vm} \quad (2)$$

where I is the discharge current, t is the discharge time, V is the potential difference during the discharging, m is the mass of active material in one electrode, and C is the specific capacitance of the electrode.

The capacitance values of HPCs in aqueous electrolyte and organic electrolyte in different current density are presented in Fig. 6. It can be found that capacitance of HPC-5 is higher than that of HPC-3 in both electrolytes, especially in organic electrolyte.

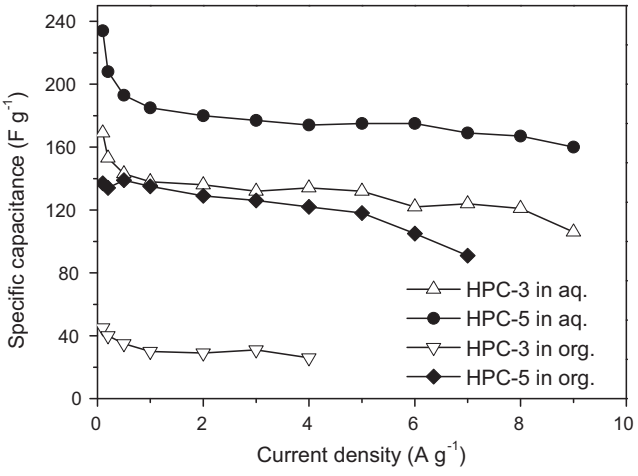

Fig. 6. Comparison of capacitance decay with increasing discharge current density of the HPCs in aqueous electrolyte (aq.) and organic electrolyte (org.).

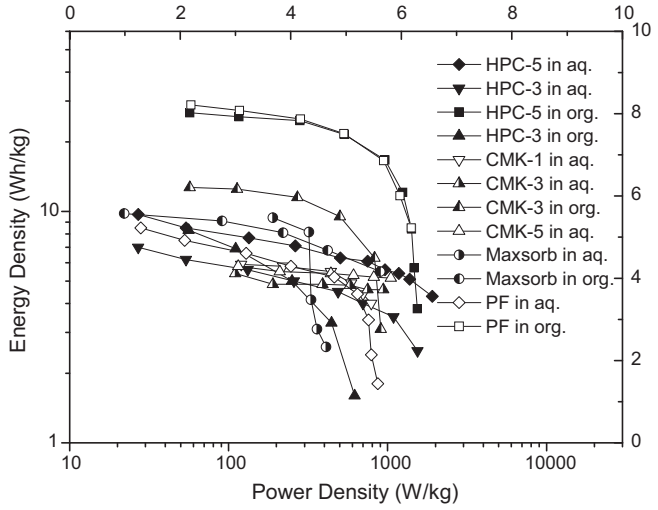

Fig. 7. Ragone plots of HPCs, ordered mesoporous carbons, Maxsorb and PF.

The capacitances of HPC-5 can reach 234 F g^{-1} in aqueous electrolyte and 137 F g^{-1} in organic electrolyte. The specific capacitance drops a bit at low current density. Because the HPCs have abundant small micropores in the frameworks derived from CO_2 adsorption isotherms, the electrolyte ions have not enough time to diffuse into all the micropores of HPCs when the current density increases. However, the specific capacitance has a good retention at high current density. The capacitance of HPC-5 maintains 160 F g^{-1} at the current density of 9 A g^{-1} in 6 M KOH aqueous, which is due to the high surface area and abundant micropores and mesopores.

The Ragone plots of HPCs, ordered mesoporous carbons, Maxsorb [11,23] and PF are shown in Fig. 7. Among these materials, HPC-5 presents the best capacitance performance in aqueous electrolyte, which maintains both high power density and energy density at high current density of 1958 W kg^{-1} and 3.5 Wh kg^{-1}. The power density and energy density of PF is smaller than those of HPC-5 which may be due to the fact that HPC-5 has a larger proportion of mesopores and maintain a better retention according to the cyclic voltammograms according to Tables 1 and 2. Maxsorb shows a high energy density, but it drops quickly when the current increases. The performances of ordered mesoporous carbons are similar due to the nearly same pore structures. In organic electrolyte, the energy densities of HPC-5 and PF are higher than those in aqueous electrolyte. HPC-5 performs both high power density and energy density. The Ragone plot of PF is nearly the same as that of HPC-5. This is due to the fact that they are derived from the same precursor and the activation degree is similar. But the yield of HPC-5 is much higher than that of PF-5. HPC-3, however, shows different property from other two samples. The energy density of HPC-3 is lower than that in aqueous electrolyte at high power density. This is because that HPC-3 shows much lower capacitance in organic electrolyte and the pore size does not match the organic electrolyte ions. Compared with Maxsorb and ordered mesoporous carbons, HPC-5 shows much higher power density and energy density.

4. Conclusions

We reported a simple method of preparation of hierarchical porous carbons derived from resols by carbonization and activation in one step, which prevents twice heating of the carbon and saves the energy and cost. Compared with conventional KOH-activated carbon such as PF, the preparation is simple and the yields of the HPC-3 and HPC-5 are high with the values of 54% and 27%. The HPCs have more abundant pore structures than the common KOH-activated carbons like CAs. The HPCs are mainly microporous characteristics with the V_{micro}/V_{total} of 91% for HPC-3 and 62% for HPC-5. The BET surface areas and total pore volumes of HPC-3/-5 are 758/2445 m^2 g^{-1} and 0.33/1.17 cm^3 g^{-1}. HPC-3 shows a narrow micropore size distribution at about 0.52 nm. For HPC-5, the pores with the diameters from 1 to 3 nm generate a lot with the average micropore size of 0.70 nm.

The HPC-5 shows good capacitance due to the high surface area, suitable micropore size and excess small mesopores which shorten the diffusion route of electrolyte ions. The capacitance of HPC-5 can reach 234 F g^{-1} in aqueous electrolyte and 137 F g^{-1} in organic electrolyte. High power density and energy density of 1958 W kg^{-1} and 3.5 Wh kg^{-1} are also obtained at high current density. Compared with CAs and PF, HPCs have both a good capacitance and a high yield. Combining the simple process of HPCs and the low cost, the porous carbon HPC-5 is a promising candidate of the electrode material for the EDLC.

Acknowledgements

We thank the Chinese National Science Foundation (No. U0734002), Shanghai Nanotechnology Promotion Center (No. 0852nm0500) and Shanghai Basic Key Program (No. 09JC1415100) for financial support.

References

[1] B.E. Conway, Electrochemical Supercapacitor: Scientific Fundamentals and Technological Applications, Plenum Publishers, New York, 1999, p. 1–220.
[2] P. Simon, Y. Gogotsi, Nat. Mater. 7 (2008) 845–854.
[3] W. Xing, F. Li, Z. Yan, G.Q. Lu, J. Power Sources 134 (2004) 324–330.
[4] R. Kötz, M. Carlen, Electrochim. Acta 45 (2000) 2483–2498.
[5] E. Frackowiak, F. Beguin, Carbon 39 (2001) 937–950.
[6] A.G. Pandolfo, A.F. Hollencamp, J. Power Sources 157 (2006) 11–27.
[7] R. Dash, J. Chmiola, G. Yushin, Y. Gogotsi, G. Laudisio, J. Singer, et al., Carbon 44 (2006) 2489–2497.
[8] K. Xia, Q. Gao, J. Jiang, J. Hu, Carbon 46 (2008) 1718–1726.
[9] M. Kaempgen, C.K. Chan, J. Ma, Y. Cui, G. Gruner, Nano Lett. 9 (2009) 1872–1876.
[10] J. Chmiola, G. Yushin, Y. Gogotsi, C. Portet, P. Simon, P.L. Taberna, Science 313 (2006) 1760–1763.
[11] E. Raymundo-Pinero, M. Cadek, F. Béguin, Adv. Funct. Mater. 19 (2009) 1032–1039.
[12] W. Xing, C.C. Huang, S.P. Zhuo, X. Yuan, G.Q. Wang, D. Hulicoua-Jurcakoua, et al., Carbon 47 (2009) 1715–1722.
[13] H. Teng, Y.-J. Chang, C.-T. Hsieh, Carbon 39 (2001) 1981–1987.
[14] J.A. Maciá-Agulló, B.C. Moore, D. Cazorla-Amorós, A. Linares-Solano, Carbon 42 (2004) 1367–1370.
[15] M.L. Martínez, M.M. Torres, C.A. Guzmán, D.M. Maestri, Ind. Crops Prod. 23 (2006) 23–28.
[16] L. Khezami, A. Ould-Dris, R. Capart, Bioresources 2 (2007) 193–209.
[17] W.T. Tsai, C.Y. Chang, S.Y. Wang, C.F. Chang, S.F. Chien, H.F. Sun, Bioresour. Technol. 78 (2001) 203–208.
[18] H. Huang, N. Kobayashi, M. Sakata, Y. Suzuki, F. Watanabe, M. Hasatani, et al., J. Mater. Cycles Waste Manage. 9 (2007) 182–187.
[19] F. Zhang, Y. Meng, D. Gu, Y. Yan, Z. Chen, B. Tu, et al., Chem. Mater. 18 (2006) 5279–5288.
[20] J. Jiang, Q. Gao, K. Xia, J. Hu, Micropor. Mesopor. Mat. 118 (2009) 28–34.
[21] J. Chmiola, C. Largeot, P. Taberna, P. Simon, Y. Gogotsi, Angew. Chem. Int. Ed. 47 (2008) 3392–3395.
[22] D. Qu, H. Shi, J. Power Sources 74 (1998) 99–107.
[23] W. Xing, S.Z. Qiao, R.G. Ding, F. Li, G.Q. Lu, Z.F. Yan, et al., Carbon 44 (2006) 216–224.